Measurement Science
and Technology

PAPER • OPEN ACCESS

Particle discrimination capabilities of lanthanum halide scintillators

To cite this article: D Rigamonti *et al* 2026 *Meas. Sci. Technol.* **37** 065501

Measurement Science and Technology

OPEN ACCESS

RECEIVED
26 September 2025

REVISED
20 December 2025

ACCEPTED FOR PUBLICATION
20 January 2026

PUBLISHED
16 February 2026

PAPER

Particle discrimination capabilities of lanthanum halide scintillators

D Rigamonti[1,*], G Guarino[2], F Camera[3], F Caruggi[1,2], C Cazzaniga[4], G Croci[2], A Dal Molin[1], N Fonnesu[5], G Gorini[2], G Grosso[1], F Guiotto[2], G Marcer[1], A Muraro[1], M Nocente[2], E Perelli Cippo[1], M Rebai[1], C Sozzi[1], L G Tedoldi[2] and M Tardocchi[1]

[1] Institute for Plasma Science and Technology, National Research Council of Italy, Milan, Italy
[2] Department of Physics, University of Milano-Bicocca, Milan, Italy
[3] Department of Physics, University of Milan, Milan, Italy
[4] UKRI-STFC, Rutherford Appleton Laboratory, Didcot OX11 0QX, United Kingdom
[5] Nuclear Department, ENEA, Via E. Fermi 45, 00044 Frascati, Rome, Italy
[*] Author to whom any correspondence should be addressed.

E-mail: davide.rigamonti@istp.cnr.it

Keywords: lanthanum halide scintillators, gamma ray spectroscopy, neutron spectroscopy, particle discrimination, fast Fourier transforms, nuclear measurements, pulse shape discrimination

Abstract

In the last few decades, lanthanum halide scintillators such as $LaBr_3$(Ce), $LaBr_3$(Ce+Sr) and $LaCl_3$(Ce) have been extensively used for gamma ray spectroscopy measurements. They offer excellent energy resolution (about 3%–4% at 662 keV) and fast scintillation time, allowing high counting rate measurements. These scintillators find applications in many research fields such as nuclear physics, astrophysics, nuclear fusion and nuclear medicine. More recently, thanks to the exploitation of the n-^{35}Cl nuclear reaction channel, $LaCl_3$(Ce) crystals have been used as neutron spectrometers. This opened up the opportunity to explore pulse shape discrimination algorithms for enabling the neutron/gamma discrimination. In this work, an innovative algorithm for particle discrimination applied to lanthanum halide scintillators is presented. The effectiveness of the algorithm has been demonstrated first on the intrinsic radioactivity measurement of the crystals, which is characterized by gamma ray emissions from ^{138}La decay and alpha decays due to actinides contamination, and then with fast neutrons. The particle discrimination feature allows for a better description of the intrinsic activity of the crystal and improved background suppression when performing gamma ray spectroscopy measurements in low cross-section measurements or in a mixed gamma-neutron radiation field.

1. Introduction

In recent decades lanthanum halide scintillators have almost completely dominated the scene of gamma ray spectroscopy measurements. This was made possible because of their high light yield, excellent energy resolution, fast scintillation decay time and high detection efficiency [1]. Their application extends from nuclear physics [2], astrophysics, nuclear medicine and more recently to nuclear fusion. An example in the nuclear fusion field is the first spectroscopic measurement on a tokamak of the gamma rays emitted by ^{3}H(^{2}H, γ)^{5}He nuclear fusion reactions [3]. In this contest, the use of a cerium doped $LaBr_3$ ($LaBr_3$(Ce)) allowed the measurement of a few gamma rays out of the 10^5 background events, leading to the assessment of the gamma to neutron branching ratio [4]. In the last years, an enhanced version of the $LaBr_3$ co-doped with cerium and strontium ($LaBr_3$(Ce+Sr)) appeared on the market. Despite a higher light yield declared, no significant improvements have been shown in terms of energy resolution. However, a significant increase in the quenching factors for charged particles has been observed for the $LaBr_3$(Ce+Sr) co-doped [5]. More recently, lanthanum chloride $LaCl_3$(Ce), which has been surpassed by the bromide version as a gamma spectrometer due to its inferior energy resolution, has been exploited for neutron spectroscopy measurements [6, 7]. In particular, it has been proposed as 2.5 MeV neutron diagnostic in deuterium nuclear fusion plasma experiments based on tokamaks, for investigating the effectiveness of external heating systems and for ion temperature assessments [8, 9]. This is made possible by exploiting the ^{35}Cl(n,p)^{35}S nuclear reaction which produces a Gaussian peak in the measured energy spectrum. The quantitative measurement of this peak, specifically its intensity, position, and width, is uniquely related to the incoming neutron energy spectrum. When dealing with neutrons, a neutron spectrometer needs to be able to discriminate the neutron events from the prompt gamma ray events produced in the experimental environment and/or in the detector itself. It has been found that the amount of cerium dopant in $LaCl_3$(Ce) affects the scintillation decay times, which in turn influences neutron/gamma identification using the pulse shape discrimination (PSD) method [6]. Increasing the amount of Ce, in fact, improves the PSD efficiency. However, this comes at the cost of a much slower scintillation decay time, preventing its use in high counting rate experiments. Furthermore, the amount of doping is determined by the $LaCl_3$ supplier's recipe and cannot be easily adjusted by the manufacturer. Non-standard methods based on fast Fourier transforms (FFTs) have been recently developed enabling efficient 2.5 MeV neutron and gamma ray discrimination with figure of merit (FOM) higher then 1, using commercial $LaCl_3$ scintillator crystals [10]. The use of a non-standard algorithm was necessary to enhance the particle discrimination capability with respect to the PSD method. This improvement is naturally reflected in a higher FOM, as described in [10].

The lanthanum halide scintillators are intrinsically radioactive due to the presence of ^{138}La isotopes and ^{227}Ac. Actinium and lanthanum are chemically analogous, and La-halide scintillators contain actinium impurities as contaminants. The ^{138}La isotope has half-life of 1.05×10^{11} years. It decays by electron capture in ^{138}Ba (with a branching ratio of 66.4 %) emitting a 1436 keV gamma ray plus 32–38 keV characteristic x-rays. The other decay process competes with a 33.6% probability, emitting a 789 keV gamma ray in coincidence with β^- emission [1]. Actinium and its daughters, instead, are responsible to α contamination which can pose limitation in rare-event experiments. In this work, intrinsic activity measurements of the three lanthanum halide crystals are presented in sections 2 and 3, together with the implementation of the FFT algorithm for α and γ particle discrimination. The promising results open up to in-beam gamma-ray spectroscopy with fast exotic beams where the background rejection is essential [2, 11]. Moreover, the use of the FFT algorithm in a mixed neutron and gamma ray flux has been investigated to reject charged particle events resulting from neutron interactions within the crystal. A description of this experiment is given in section 4, while the results are presented in section 5. Section 6 is dedicated to discussion and conclusions.

2. Experimental setup for intrinsic activity measurements and signal processing

The FFT-based algorithm for particle discrimination has been initially tested on intrinsic activity measurements performed at the CNR-ISTP laboratories in Milan, using three samples of lanthanum halide scintillators: $LaBr_3$(Ce), $LaBr_3$(Ce+Sr) and $LaCl_3$(Ce). The scintillators used are commercially available and were manufactured by Luxium Solutions [12] with nominal dopant concentrations. The properties of the samples are summarized in table 1. The scintillators have been individually coupled to a photomultiplier tube (model R9420-100-10) manufactured by Hamamatsu [13] and biased with –800 V. The photomultiplier tube serves as photo-sensor converting the scintillation light into an electrical signal whose amplitude is proportional to the energy deposited inside the scintillator. Then the output signal was directly fed into a DT5730 CAEN digitizer with 14bit resolution and 500 Msps [14] able to store every waveform above a selected threshold. Data have been analyzed off-line. For each waveform, its integral over a selected gate 200 ns long was calculated to build the measured energy spectrum (see an example in figure 5). The Fourier Transform was computed by a Python code implementing a FFT routine allowing to calculate the amplitude (magnitude) of the frequencies composing the waveforms. Example of the FFT amplitude spectrum calculated for the gamma and alpha events are shown in figure 1. The particle discrimination algorithm is based on the assessment of a quantitative parameter, here called amplitude Fourier shape discrimination (AFSD), which is the analogous of the PSD value used in the standard PSD method (PSD). The AFSD is calculated as the ratio between the integrals of the FFT amplitude spectrum over two appropriately selected gates. The 2D scatterplot of the ASFD values as a function of the associated deposited energy allows for the identification and selection of events attributable to a specific particle type (see figure 2). The goodness of the particle discrimination capability is assessed by the FOM of the AFSD spectrum that is the projection of the 2D scatterplot of the AFSD values. Here the FOM is defined as

$$\mathrm{FOM} = \frac{d}{\mathrm{FWHM}_\gamma + \mathrm{FWHM}_\alpha}$$

Table 1. Summary of the properties of the scintillators employed in this work.

Scintillator	Size $\phi \times$ h (mm^2)	Light yield ph. (MeV)	Decay time (ns)
$LaBr_3(Ce)$	25.4 × 16.9	63 000	16
$LaBr_3(Ce{+}Sr)$	25.4 × 25.4	73 000	25
$LaCl_3(Ce)$	25.4 × 25.4	49 000	28

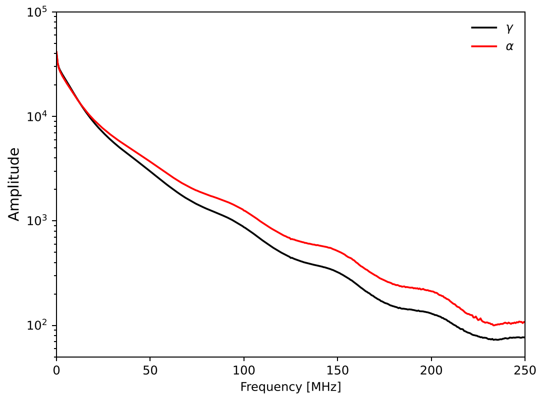

Figure 1. FFT amplitude spectrum of the averaged waveforms of gamma and alpha particles.

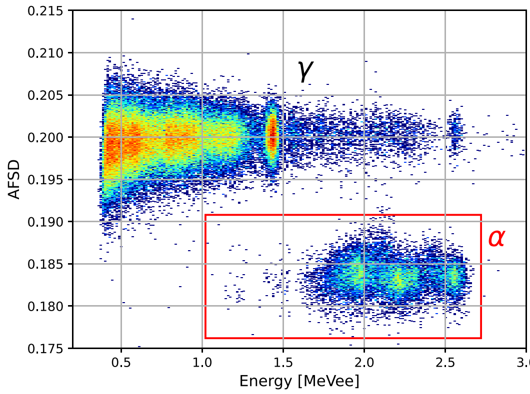

Figure 2. 2D scatterplot of the AFSD values related to internal activity measurement of the $LaBr_3(Ce)$ scintillator crystal. The red rectangle represents the alpha events due to actinide contamination, while band in the top represents gamma ray events.

where $FWHM_\gamma$ and $FWHM_\alpha$ are the full width at half maximum (FWHM) of the Gaussian peaks in the AFSD spectrum related to gamma events, and alpha events, respectively, and d is their distance. Details on the algorithm can be found at this reference [10].

3. Results of the intrinsic activity measurements

The 2D scatterplots of the AFSD values, together with the related AFSD spectra, have been realized for the three scintillator crystals (see figure 3 for the AFSD spectrum in the $LaBr_3(Ce)$ case) and used to assess the FOM (see table 2). $LaCl_3(Ce)$ and $LaBr_3(Ce)$ scintillator crystals resulted to have the same FOM of about 2.1, which translates in a superior separation of the γ and α particles contributions, with respect to the third crystal (see figure 4). Table 2 also provides a comparison between the FOM calculated using the FFT method and that obtained with the standard PSD algorithm. It can be clearly seen that the FOM from the FFT method is significantly higher, reflecting the improved particle discrimination capability achieved with this approach. In lanthanum halide scintillators, the alpha contribution is due to the presence of ^{227}Ac and the alpha decays of its daughters ^{223}Ra, ^{227}Th, ^{211}Bi, ^{219}Rn, ^{215}Po [15]. In particular, the ^{215}Po isotope emits an alpha particle with an energy of $E_\alpha = 7.3861$ MeV [15], which, according to [15], corresponds to the third peak in the alpha spectrum (see figures 4 and 5). In the case of the $LaBr_3(Ce)$ scintillator, this peak appears at approximately 2.55 MeVee in the measured energy spectrum. The ratio between the peak position in the measured spectrum and the energy of the

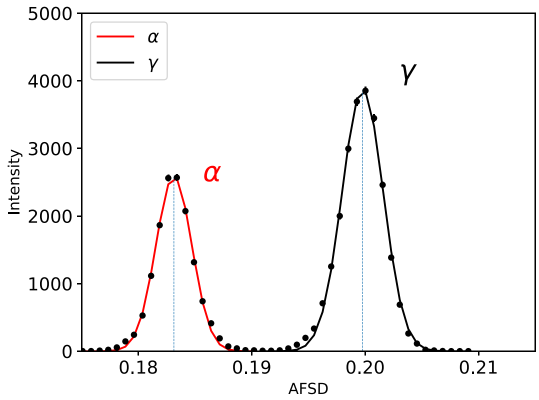

Figure 3. AFSD spectrum obtained with $LaBr_3$(Ce) scintillator crystal with an energy threshold of 1.0 MeVee.

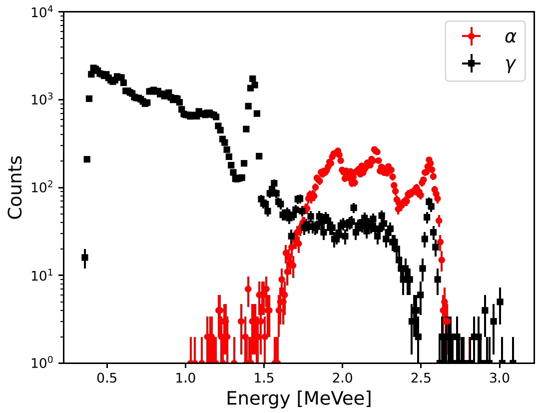

Figure 4. Energy spectra measured from the internal radioactivity of the $LaBr_3$ scintillator, categorized by particle type.

Table 2. Summary of the FOM obtained with the scintillator crystals with both the FFT method and the standard PSD method.

Scintillator	Energy threshold	FOM (FFT)	FOM (PSD)
$LaBr_3$:(Ce)	1.0 MeV	2.09 ± 0.02	0.80 ± 0.04
$LaBr_3$:(Ce+Sr)	1.0 MeV	0.89 ± 0.01	0.85 ± 0.04
$LaCl_3$:(Ce)	1.0 MeV	2.08 ± 0.01	1.00 ± 0.02

alpha particle provides the quenching factor of the light yield. It has been found that the two scintillators doped with Cerium have the same quenching factor about 0.34 ± 0.01, while the $LaBr_3$ doped with Cerium and Strontium has a significantly higher quenching factor (0.46 ± 0.1), as exhibited in figure 5.

4. 14 MeV neutron measurements at the Frascati neutron generator (FNG)

14 MeV neutron measurements with a $LaBr_3$(Ce) scintillator crystal have been recently performed at the ENEA FNG. Here, the neutrons are produced via deuterium–tritium (DT) nuclear fusion reactions ^{3}H(d, n)^{4}He. Deuterons are accelerated up to 230 keV and 1 mA current onto a Titanium–tritiade target (TiT) resulting in a 14 MeV neutron emission rate up to 10^{11} s^{-1} emitted over 4π [16]. The absolute neutron yield is provided within an uncertainty of 3% by a silicon detector subtending a small and well known solid angle measuring the α particles produced by DT nuclear fusion reactions, cross-calibrated with activation foils measurements [17]. The TiT target is kept a few meters away from the accelerating tube end and from the bunker walls, reducing the neutron scattering component. A $LaBr_3$(Ce) scintillator crystal with dimension $25.4 \times 16.9\,mm^2$ ($\phi \times h$) was coupled to a photomultiplier tube (model R9420-100-10) provided by Hamamatsu [13]. A reduced bias voltage of -600 V was applied to extend the detector's dynamic range, enabling it to manage the intense signals produced by 14 MeV neutrons while keeping the signal amplitude within the 2 V input range of the CAEN DT5730 digitizer. Signal processing was carried out as described in the previous section

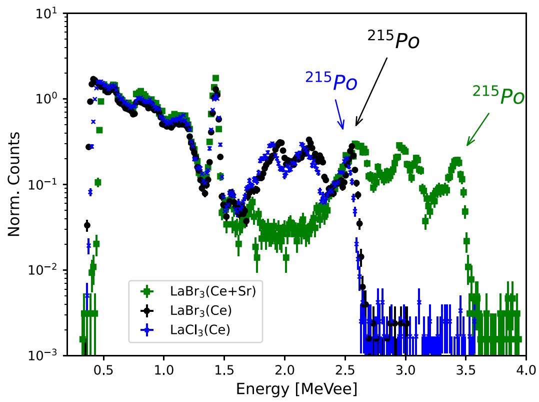

Figure 5. Energy spectra due to internal radioactivity of the three scintillator samples.

Table 3. List of the element, the nuclear reactions, the half-lives of the produced radioisotope and the gamma ray lines used for the calibration.

Element	Nuclear reaction	$t_{1/2}$	E_γ [MeV]
^{27}Al	^{27}Al(n,α)^{24}Na	14.99 h	1.368625; 2.75403
^{54}Fe	^{54}Fe(n,p)^{54}Mn	312 d	0.83485

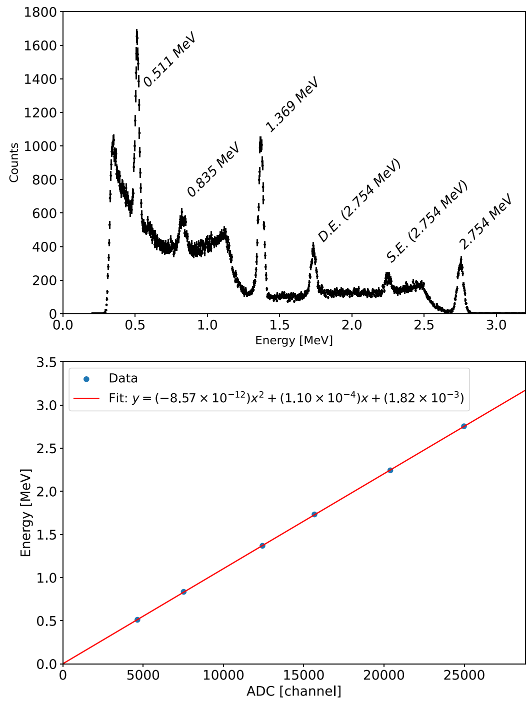

Figure 6. Calibration measurement with the LaBr$_3$(Ce) scintillator crystal at FNG (top) and the second-degree polynomial fit (bottom). The peaks labeled as S.E. (2.754 MeV) and D.E. (2.754 MeV) refer to the single-escape and double-escape peaks of the 2.754 MeV gamma-ray line, respectively.

Calibration measurements have been performed exploiting the gamma ray lines due to neutron activation of ^{27}Al and ^{54}Fe present in the FNG hall and the 0.511 MeV gamma ray line due to positron–electron annihilation (see figure 6). The list of the gamma rays used for the calibration, together with the nuclear reactions involved and half-lives of the produced radionuclide are listed in table 3. In the measured spectrum showed in figure 6-top, the peaks labeled as S.E.(2.754 MeV) and D.E.(2.754 MeV) refer to the single escape peak and the double escape peak, respectively. The calibration measurements were taken 18 hours after the neutron generator was turned off. In the assumption that in 5 half-lives nearly the most of the radionuclides have decayed, only gamma rays emitted by radionuclides with half

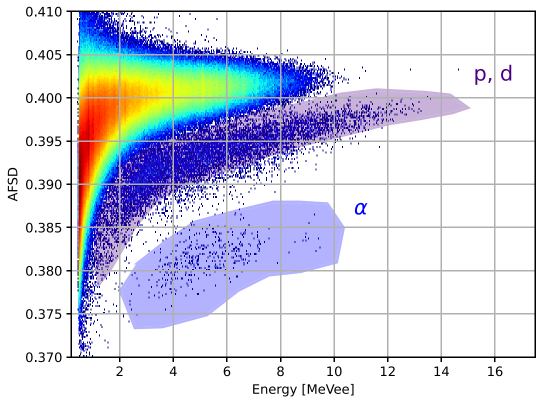

Figure 7. 2D scatterplot of the AFSD values obtained from the 14 MeV neutron measurement and analyzed using the FFT algorithm. Events within the indigo region correspond to secondary protons and deuterons produced by neutron interactions with the $LaBr_3$(Ce), while events within the blue region are associated with secondary alpha particles.

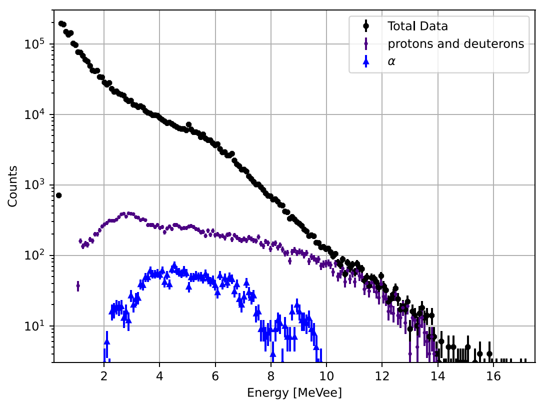

Figure 8. Total energy spectrum measured by the $LaBr_3$(Ce) scintillator crystal during the 14 MeV neutron irradiation (black circles), together with the energy spectrum corresponding to secondary protons and deuterons (indigo dots) and alpha particles (blue triangle up marker) produced by neutrons inside the scintillator.

lives slower than 3.6 h can be significantly distinguishable from the environmental background. The neutron measurement has been performed with the $LaBr_3$(Ce) detector placed a few meters from the TiT target to decrease the count rate and, consequently, the pile-up probability. The neutron measurement lasted 5 min with a neutron yield of 5×10^{-9} n s^{-1}, resulting in a detector count rate of about 13 kHz with a pile-up probability lower than 1%. The 2D scatterplot of the AFSD values has been produced to select the events related to charged particles produced by nuclear reactions between the neutrons and the nuclei composing the scintillator (see figure 7) and to build the corresponding energy spectra (see figure 8).

5. Results of the neutron measurements and data interpretation

Data analysis took advantage from the progresses done in [18, 19] in which the response of a $LaBr_3$(Ce) scintillator has been calculated via MCNP simulations [20, 21] and compared to measurements. It has been found that the total measured spectrum shown in figure 8 is dominated by γ events induced by neutrons inside the crystal. For energies higher than 5 MeVee, instead, the proton production, which is mainly due to n+^{79}Br interactions, contributes the most. This causes a change of slope in the spectrum that can be noted both in figure 8 and in the reference paper [19]. Deuterons and alpha particles are also generated, mainly from neutron interaction with ^{79}Br and ^{81}Br isotopes, but with lower probability. In this paper, the FFT method has been used to identify and select the events related to secondary charged particles created inside the crystal (see figure 7). The achieved energy spectra have been compared to simulations taking into account the quenching effect of the scintillation light yield. The electron equivalent energy has been calculated using the empirical formula (equation (1)) described by Birks' law

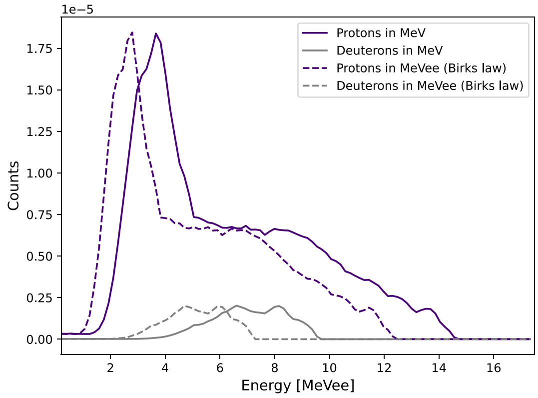

Figure 9. Protons and deuterons spectra calculated with MCNP in indigo and gray lines, respectively and the corresponding spectra in MeV electron equivalent energy calculated using Birks law in indigo and gray dashed lines.

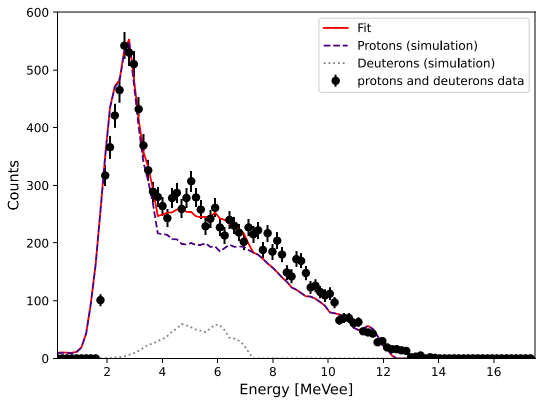

Figure 10. Protons and deuterons spectra calculated with MCNP (indigo and gray dashed lines, respectively), summed together to fit the data (red line and black circles).

[22, 23] in which the light yield of the scintillator depends on the particle energy and the particle stopping power $\mathrm{d}E/\mathrm{d}x$:

$$\frac{\mathrm{d}L}{\mathrm{d}x} = \frac{S\frac{\mathrm{d}E}{\mathrm{d}x}}{1 + kB\frac{\mathrm{d}E}{\mathrm{d}x}} \tag{1}$$

Here, $\mathrm{d}L/\mathrm{d}x$ is the scintillation yield density, S is the scintillation efficiency, $\mathrm{d}E/\mathrm{d}x$ is the stopping power in the $LaBr_3$(Ce) scintillator calculated for protons, deuterons and alpha particles using SRIM code [24–26] and, finally, kB is the Birks coefficient. In this specific calculation, S and kB coefficients have been assumed to be 1 and 0.0009 cm MeV^{-1}, respectively, resulting in a quenching factor compatible with the one obtained during the internal activity measurements and in [18, 19]. The calculated proton and deuteron spectra (see figure 9) were summed without adjusting their relative intensities from the simulations, and the result was used to numerically fit the corresponding data (see figure 10). In this case, it was assumed that the energy deposition density of protons and deuterons is much more similar to each other than to that of alpha particles, resulting in comparable waveforms and FFT spectra. From a qualitative perspective, the spectral shape of secondary protons and deuterons agrees with the simulations. A first attempt to describe the secondary alpha spectrum resulting from neutron interactions within the crystal has been carried out using both MCNP and GEANT4 simulations (see figure 11). Although the secondary proton spectra computed by both MCNP and GEANT4 are comparable, the simulated spectra of the secondary alpha particles show clear differences. In this case, a reasonable agreement between measurements and simulations was achieved, although discrepancies may be attributed to uncertainties in the cross-section libraries. Moreover, GEANT4 simulations predict an alpha peak that is also visible in the measurements, although with an energy shift of approximately 1 MeV.

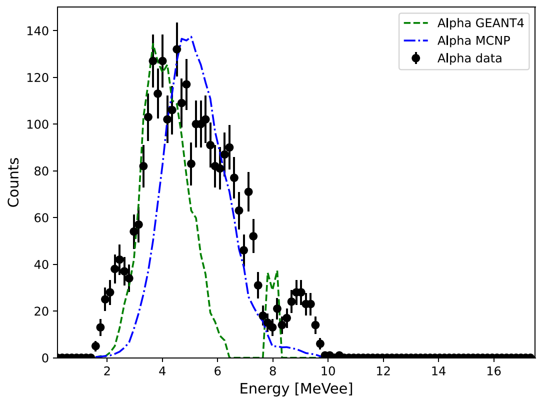

Figure 11. Alpha spectra calculated with both MCNP and GEANT4 simulations (blue and green dashed lines, respectively) and compared to the data (black circles).

6. Discussion and conclusions

The particle discrimination capability of the $LaBr_3$(Ce), $LaBr_3$(Ce+Sr) and $LaCl_3$(Ce) scintillators crystals has been demonstrated by using a non-standard algorithm based on FFT. It has been found that the activator amount and species drastically affect the particle discrimination capability of the instrument. This is the case of the $LaBr_3$(Ce+Sr) which has a much lower FOM with respect to the one obtained by the other two scintillators activated with only Cerium. Moreover, although the addition of strontium was expected to increase the scintillation light yield, it does not lead to the desired improvement in energy resolution for gamma rays measurements [5]. Its most distinctive feature is the higher quenching factor for charged particles which translates in higher energy resolution for charged particles. Based on these results, we propose to exploit a $LaCl_3$(Ce+Sr) for 2.5 MeV neutron spectroscopy measurements on deuterium fusion plasma. In fact, this detector would combine the spectroscopic reaction channel ^{35}Cl(n,p)^{35}S for neutron detection in deuterium plasma with improved energy resolution. Moreover, although the addition of strontium results in a lower FOM under the same energy threshold conditions, an higher quenching factor would allow for an increased energy threshold, thereby improving the separation of the neutron peak from gamma rays. During the laboratory measurements, it has been observed that the performances of the FFT method in discriminating the different particles can be affected by electronic noise. In a few occasions, an high frequency noise has been observed in the digitized waveforms. This prevented the integration of the full range of available frequencies for the AFSD calculation, limiting the analysis to a restricted sub-range. As expected, a worst FOM equal to 1.4 ± 0.02 instead of 2.1 ± 0.02 was obtained, which, however, did not prevent the particle discrimination. Although the origin of the high frequency electronic noise remains unclear, the noise disappeared after replacing the digitizer with a Teledyne SP Devices [27] model. The installation of a 2.5 MeV neutron spectrometer based on $LaCl_3$ scintillator crystal on nuclear fusion experiments, such as the JT-60SA and MASTu tokamaks has been proposed within the EUROfusion WPSA and WPTE work packages. The role of the $LaCl_3$ based diagnostic is the measurement along a collimated line of sight of the 2.5 MeV neutron energy spectrum directly emitted by deuterium–deuterium nuclear fusion reactions. The energy of the neutrons is linked to the energy of the reactants and could provide the ion temperature of the plasma and information on the effectiveness of external heating systems [8, 9]. Thereby, the use of the FFT method in highly noisy environments, such as those of a nuclear fusion tokamak experiment, requires further investigations. In this paper, the enhanced particle discrimination capability of a $LaBr_3$(Ce) scintillator crystal has been demonstrated with intrinsic activity (γ and α) measurements and with 14 MeV neutrons. The promising results open up for improvements in nuclear structure and nuclear astrophysics experiments at rare-isotope facilities. In particular, for in-beam gamma-ray spectroscopy measurements with fast exotic beams that require background rejection. The 14 MeV neutron measurements, instead, allowed the identification of the secondary charged particle produced by neutrons inside the crystal. Although the most effective way to reduce the neutron-induced background events in gamma ray spectroscopy experiments conducted in a harsh mixed neutron and gamma ray environment is undoubtedly the use of a neutron attenuator, the implementation of a particle discrimination algorithm can improve rare gamma ray measurements. This is particularly relevant for the γ_0 and γ_1 emitted by ^{3}H(^{2}H, γ)^{5}He nuclear fusion reactions measurements for the assessment of the fusion power [3, 4].

Data availability statement

The data cannot be made publicly available upon publication because they are not available in a format that is sufficiently accessible or reusable by other researchers. The data that support the findings of this study are available upon reasonable request from the authors.

Author contributions

D Rigamonti 0000-0003-0183-0965
Conceptualization (lead), Formal analysis (equal), Investigation (lead), Methodology (equal), Supervision (equal), Writing – original draft (lead)

G Guarino 0009-0000-6286-1111
Formal analysis (lead), Investigation (equal), Software (lead), Visualization (equal)

F Camera 0000-0003-1731-4834
Conceptualization (equal), Investigation (equal), Supervision (equal), Validation (equal)

F Caruggi 0000-0002-5480-1327
Conceptualization (equal), Investigation (equal), Validation (equal)

C Cazzaniga
Investigation (equal), Methodology (equal), Supervision (equal), Writing – review & editing (equal)

G Croci 0009-0004-3302-4209
Data curation (equal), Formal analysis (equal), Supervision (equal), Validation (equal)

A Dal Molin 0000-0003-0471-1718
Investigation (equal), Methodology (equal), Supervision (equal), Validation (equal), Writing – review & editing (equal)

N Fonnesu 0000-0002-2800-0040
Investigation (equal), Methodology (equal)

G Gorini 0000-0002-4673-0901
Supervision (equal)

G Grosso 0009-0003-6695-152X
Methodology (equal), Supervision (equal)

F Guiotto 0000-0001-6014-918X
Data curation (equal), Formal analysis (equal), Investigation (equal), Methodology (equal), Software (equal)

G Marcer 0000-0002-1170-5925
Investigation (equal), Validation (equal), Writing – review & editing (equal)

A Muraro 0000-0002-4570-4576
Investigation (equal), Methodology (equal), Validation (equal)

M Nocente 0000-0003-0170-5275
Investigation (equal), Methodology (equal)

E Perelli Cippo 0000-0002-8151-3427
Investigation (equal), Methodology (equal), Validation (equal)

M Rebai 0000-0002-0247-9073
Investigation (equal), Methodology (equal)

C Sozzi 0000-0001-8951-0071
Investigation (equal), Supervision (equal)

L G Tedoldi 0009-0001-7664-2291
Data curation (equal), Formal analysis (equal), Investigation (equal), Methodology (equal), Visualization (equal)

M Tardocchi 0000-0001-8443-1809
Investigation (equal), Methodology (equal), Supervision (equal), Validation (equal)

References

[1] Chattopadhyay D, Sharma S and Saha Sarkar M 2021 Reduction of the effect of internal activity in LaCl 3: Ce scintillator *J. Instrum.* **16** 06025

[2] Crespi F *et al* 2009 Alpha–gamma discrimination by pulse shape in LaBr3: Ce and LaCl3: Ce *Nucl. Instrum. Methods Phys. Res. A* **602** 520–4

[3] Rebai M *et al* 2024 First direct measurement of the spectrum emitted by the $^{3}H(^{2}H,\gamma)^{5}$He reaction and assessment of the relative yield γ_1 to γ_0 *Phys. Rev. C* **110** 014625

[4] Dal Molin A *et al* 2024 Measurement of the gamma-ray-to-neutron branching ratio for the deuterium-tritium reaction in magnetic confinement fusion plasmas *Phys. Rev. Lett.* **133** 055102

[5] Panwar S, Mazumdar I, Sariyal R, Ranga V, Patel S, Chavan P and Gourishetty A 2020 Characterization of a Sr co-doped LaBr: (Ce) detector for γ -ray spectroscopy *Nucl. Instrum. Methods Phys. Res. A* **982** 164567

[6] Vuong P Q, Kim H, Luan N T and Kim S 2021 Neutron spectroscopy using pure LaCl3 crystal and the dependence of pulse shape discrimination on Ce-doped concentrations *Nucl. Eng. Technol.* **53** 3784–9

[7] Taggart M and Henderson J 2020 Fast-neutron response of LaBr3(Ce) and LaCl3(Ce) scintillators *Nucl. Instrum. Methods Phys. Res. A* **975** 164201

[8] Kormilitsyn T M, Obudovsky S Y, Rodionov R N, Pankratenko A V, Dzhurik A S, Kashchuk Y A and Krasilnikov A V 2021 Novel LaCl3(Ce)-based spectrometer for deuterium plasma neutron diagnostics *Rev. Sci. Instrum.* **92** 043528

[9] Pankratenko A *et al* 2023 Analysis of the LaCl3(Ce) scintillator response function to fast neutrons *Nucl. Instrum. Methods Phys. Res. A* **1052** 168282

[10] Rigamonti D *et al* 2024 A chlorine based detector (LaCl3(Ce)) for 2.5 MeV neutron spectroscopy in deuterium nuclear fusion plasmas with enhanced particle discrimination algorithm *Meas. Sci. Technol.* **36** 015907

[11] Weisshaar D *et al* 2008 LaBr3:Ce scintillators for in-beam gamma-ray spectroscopy with fast beams of rare isotopes *Nucl. Instrum. Methods Phys. Res. A* **594** 56–60

[12] Luxium solutions (available at: https://luxiumsolutions.com/)

[13] Hamamatsu photonics (available at: https://www.hamamatsu.com/jp/en.html)

[14] Caen s.p.a (available at: https://www.caen.it/)

[15] Wolszczak W and Dorenbos P 2017 Shape of intrinsic alpha pulse height spectra in lanthanide halide scintillators *Nucl. Instrum. Methods Phys. Res. A* **857** 66–74

[16] Martone M, Angelone M and Pillon M 1994 The 14 MeV Frascati neutron generator *J. Nucl. Mater.* **212-215** 1661–4

[17] Pietropaolo A *et al* 2018 The Frascati neutron generator: a multipurpose facility for physics and engineering *J. Phys.: Conf. Ser.* **1021** 012004

[18] Rigamonti D *eta l* 2017 Characterization of a compact LaBr3(Ce)detector with Silicon photomultipliers at high 14 MeV neutron fluxes *J. Instrum.* **12** C10007

[19] Cazzaniga C *et al* 2015 Response of LaBr3(Ce) scintillators to 14 MeV fusion neutrons *Nucl. Instrum. Methods Phys. Res. A* **778** 20–25

[20] Waters L S 2002 MCNPX™ user's manual, version 2.3.0 *Technical Report* LA-UR-02-2607 Los Alamos National Laboratory Los Code Version 2.3.0

[21] Goorley J T *et al* 2013 Initial MCNP6 release overview - MCNP6 version 1.0 *Technical Report* LA-UR-13-22934 Rev. 1 Los Alamos National Laboratory Los

[22] BIRKS J 1964 *The Theory and Practice of Scintillation Counting International Series of Monographs in Electronics and Instrumentation* (Pergamon)

[23] Birks J B 1951 Scintillations from organic crystals: specific fluorescence and relative response to different radiations *Proc. Phys. Soc. A* **64** 874

[24] Ziegler J F and Biersack J P 1985 *The Stopping and Range of Ions in Matter* pp 93–129

[25] Ziegler J F 2004 SRIM-2003 *Nucl. Instrum. Methods Phys. Res. B* **219-220** 1027–36

[26] Ziegler J F, Ziegler M and Biersack J 2010 SRIM–The stopping and range of ions in matter (2010) *Nucl. Instrum. Methods Phys. Res. B* **268** 1818–23

[27] Teledyne sp devices www.spdevices.com/